Thermal conductivity of semiconductor disk lasers for more accurate heat management

YANBIN MEN, FANG WEN, SHUMIN ZHANG[*]
College of Physics and Information Engineering, Hebei Normal University, Shijiazhuang, China

Accurate heat management is crucial for a high-power, good beam quality semiconductor disk laser because the emitting wavelength, the resonant periodic gain structure, and the microcavity modes of the laser are all temperature sensitive, and ideal performance could be achieved only if the above three elements are carefully controlled and coincided at the working temperature. The gain chip of a semiconductor disk laser is consisted of two nanostructures: the multiple quantum wells and the distributed Bragg reflector. In this work, three theoretical methods, in which various nanoscale effects are considered, are employed to calculate the thermal conductivity of similar multilayer nanostructures. By referencing to reported experiments, the one more agree with measured data is picked out to compute thermal conductivities of multiple quantum wells and distributed Bragg reflector, and the results are compared with bulk values.

1. Introduction

Semiconductor disk lasers (SDLs) take advantages of both semiconductor surface emitting lasers and solid state disk lasers, and can produce high power and good beam quality simultaneously [1-3]. SDLs were well developed in the past decade, and had been successfully applied in diverse fields such as laser display [4], spectroscopy [5], life science [6], military [7], therapeutic applications [8], forensic medicine [9], and so on.

The typical configuration of a SDL is shown in Fig. 1. The gain chip, consisted of the distributed Bragg reflector (DBR), the multiple quantum wells (MQWs), and a window layer, is epitaxially grown on a substrate, and subsequently bonded to a heatsink. The DRB and the output coupler (OC) form the laser cavity, MQWs provide gain for the laser, and the window layer prevent carriers from nonradiative recombination at surface. Pumping source is focused onto the gain chip, absorbed by the barriers of MQWs, and the generated carriers are captured into wells and emit stimulated radiation.
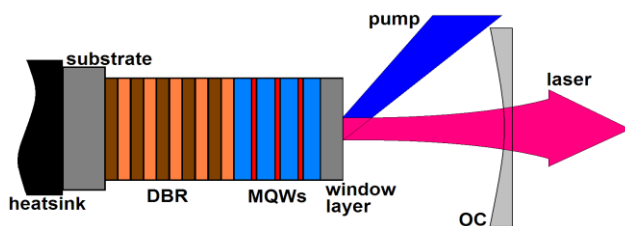
Fig. 1. Configuration of a typical SDL

When the SDL is working, DBR at bottom of the chip and the semiconductor-air interface at top of the chip form a microcavity in the laser, and there is a laser standing wave between them. MQWs should be situated at the antinodes of the standing wave, satisfied the so-called resonant periodic gain (RPG) structure [10], so to obtain the gain of laser as much as possible. Meanwhile, together with the external cavity, the microcavity modes also limit the output laser wavelength. It is clear that ideal performance could be achieved only if the MQWs emitting wavelength, the RPG structure, and the microcavity modes coincided at the working temperature, as can be seen from Fig. 2. Unfortunately, the above three elements are all temperature sensitive, so they must be carefully controlled in a high power, good beam quality SDL, and this means, thermal management play a more important role for a SDL.
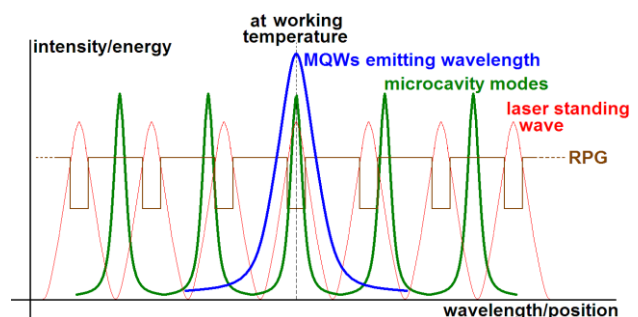
Fig. 2. Schematics of MQWs emitting wavelength, microcavity modes, laser standing wave and RPG structure

It can be seen form Fig. 1, the gain chip of a semiconductor disk laser is consisted of two nanostructures: the MQWs and the DBR. Thermal analysis about SDLs in the previous works treated these two parts as bulk material, calculated thermal conductivities of MQWs and DBR through the weighted average of the bulk

values [11-14], and they may underestimate the temperature rise in the active region.

This work uses three theoretical methods, in which various nanoscale effects are considered, to simulate thermal conductivities of GaAs/AlAs multilayer nanostructures. By referencing to reported experiments, the one more agree with measured data is picked out to compute thermal conductivities of MQWs and DBR used in SDLs, and the results are compared with bulk values.

2. Comparison of different theoretical methods

2.1. Theoretical methods

Method 1: L.H. Liang et al had studied the size dependence of thermal conductivity in nanoscale semiconductor systems and derived an analytical formula including surface scattering and size confinement effects of phonon transport [15]. By taking into account the intrinsic size effects of phonon velocity, mean free path (MFP) and surface scattering effects, the size-dependent thermal conductivity was obtained as

$$\frac{\kappa_L}{\kappa_b} = p \exp(-\frac{l_0}{L})[\exp(\frac{-(\alpha-1)}{L/L_0})]^{3/2} \qquad (1)$$

Subscripts L and b mean the nanostructure and the corresponding bulk material. L is the size of nanostructures, such as the diameter of nanowires or the thickness of thin films. L_0 is a critical size at which almost all atoms of a crystal are located on its surface. $L_0=2(3-d)w$ with the atomic/molecular diameter w and the dimension $d=0, 1, 2$ for nanoparticles, nanowires and thin films, respectively. p is a factor reflecting the surface roughness, $0<p<1$. Larger value of p corresponds to smaller roughness, thus more probability of specular scattering, vice versa, smaller p corresponds to more probability of diffusive scattering. l_0 is the phonon MFP in the Debye model at room temperature and assumed to be a constant. $\alpha=\sigma_s^2/\sigma_i^2$ is a material constant with σ_s^2 and σ_i^2 corresponding to the root mean square displacement of

surface atoms of a crystal and that of atoms within the crystal, respectively. $\alpha=2S_v/(3R)+1$, $S_v=S_m-R$ and $S_m=H_m/T_m$ with the bulk melting entropy S_m, enthalpy H_m and temperature T_m. R is the ideal gas constant.

Method 2: A simple analytical expression with a combination of acoustic mismatch model (AMM) and diffuse mismatch model (DMM) for thermal boundary resistance, joining a model expansion of Boltzmann equation was proposed by F.X. Alvarez et al [16]. It can predict in-plane and cross-plane values of thermal conductivities of superlattices. The total thermal resistivity of the material was split into two parts: the first one due to the change in the equilibrium distribution of phonons caused by their large MFP, called intrinsic layer conductivity (ILC), and the second one due to the crossing of the interface, traditionally called thermal boundary resistance (TBR). The main difference between F.X. Alvarez's proposal and others previously literature was that F.X. Alvarez assumed that the change in the thermal conductivity of total device was partially due to the size influence on the ILC while other models assumed classical Fourier limit for this term. This splitting produced an analytic approximate expression for the total thermal conductivity.

The ILC can be obtained from a moment expansion of Boltzmann equation

$$\kappa_{ILC} = \frac{\kappa_b L_{eff}^2}{2\pi^2 l_0^2}[\sqrt{1+(\frac{2\pi l_0}{L_{eff}})^2} -1] \qquad (2)$$

where κ_b is bulk thermal conductivity, l_0 the MFP of carriers and L_{eff} the effective length of system

$$L_{eff} = (1-\Gamma)L_1 + (1-\Gamma)\Gamma L_2 +\cdots+ (1-\Gamma)\Gamma^{N-2}L_{N-1} + \Gamma^{N-1}L_N \qquad (3)$$

where $L_n=nL_{lay}$ (n=1, 2, . . . , N) are the distance between the starting interface on layer 1 and the ending interface on layer n and N is the total number of layers if all layers have the same thickness L_{lay}.

In superlattices, phonons cross alternatively 12 and 21 interfaces, the net transmission coefficient Γ_{ij} from material i to material j is [17]

$$\Gamma_{ij} = p\Gamma_{Sij} + (1-p)\Gamma_{Dij} = p\times 2\int \tau_{Sij}(\mu_i)\mu_i d\mu_{1i} + (1-p)\int \tau_{Dij}(\mu_i)\mu_i d\mu_{1i} \qquad (4)$$

and the average transmission coefficient Γ is defined as

$$\Gamma = \frac{\Gamma_{12} + \Gamma_{21}}{2} \qquad (5)$$

where the adjustable specularity parameter p ($0\leq p\leq 1$) is used to consider partially specular and diffuse interfaces. $\mu_i=\cos\theta_i$ and θ_i is the incident angle of phonons in medium i. Calculation of μ_i and τ_{Sij} can be found in reference [16].

If $\kappa_{1, 2}$ are the ILCs of layers 1 or 2, respectively, intrinsic in-plane or cross-plane superlattice thermal

conductivities only differ in the way the individual conductivities are combined, namely

$$\kappa_{IP} = \frac{\kappa_1 L_1 + \kappa_2 L_2}{L_1 + L_2} \qquad (6)$$

$$\kappa_{CP} = \frac{L_1 + L_2}{L_1 / \kappa_1 + L_2 / \kappa_2} \qquad (7)$$

Through expression (6), the ILC of superlattice, i.e., the in-plane superlattice thermal conductivity can be

obtained. It should be noted that expression (7) only gives the ILC part of cross-plane superlattice thermal conductivity and another part, TBR, must be added in expression (7) to calculate the cross-plane superlattice thermal conductivity as

$$\kappa_{CP+R} = \frac{\kappa_{CP}}{1 + \frac{2\kappa_{CP}R_m}{L_1 + L_2}} \qquad (8)$$

where R_m will be given by the following expression (9).

As to the TBR, two different models, AMM and DMM, are widely used to predict it. A real boundary, however, is a combination of both models with weights p and $1-p$, where $p=1$ corresponding to the pure specular and $p=0$ to the pure diffuse transmissivities. From the transmission coefficients Γ_{ij} determined in (4), the TBRs from material i to material j, R_{ij}', can be obtained by using [17]

$$R_{ij}' = \frac{4\pi^2\hbar^3 v_i^2}{k_B^4 \Gamma_{ij} T_i^3} \frac{1}{\int_0^{x_{Di}} x^4 e^x / (e^x - 1)^2 dx} \qquad (9)$$

where k_B and $\hbar$ are Boltzmann and Planck constants, T_i is the temperature of the material i at the interface and $x_{Di} = \theta_D / T_i$, where θ_D is its Debye temperature.

The above expression of TBR includes the resistive contributions of two layers of width L_1 and L_2, and the MFP of phonons in their respective materials. If one wants to calculate the single contribution of the interface, the contribution of these layers to the total resistance should be subtracted as

$$R_{ij} = R_{ij}' - \frac{L_1}{\kappa_{b1}} - \frac{L_2}{\kappa_{b2}} \qquad (10)$$

with κ_{bi} being the bulk thermal conductivity of medium i.

Method 3: Alan J.H. McGaughey et al developed an analytical model for the size-dependence of thin film and nanowire thermal conductivity [18]. The model includes mode-dependence of the phonon lifetime resulting from phonon-phonon and phonon-boundary scattering, contains no fitting parameters and only requires the bulk lattice constant, bulk thermal conductivity, and an acoustic phonon speed as inputs. The in-plane and cross-plane thermal conductivities of thin film are

$$\frac{\kappa_{IP}}{\kappa_b} = \frac{4}{7} - \frac{3}{28}\xi + \frac{3}{14}\xi^2 + \frac{1}{2}\xi\ln(1+\frac{1}{\xi}) - \frac{3}{14}\xi^3\ln(1+\frac{1}{\xi}) - \frac{4}{7\sqrt{\xi}}\arctan\sqrt{\xi} \qquad (11)$$

$$\frac{\kappa_{CP}}{\kappa_b} = \frac{6}{7} + \frac{3}{14}\xi - \frac{3}{7}\xi^2 + \frac{3}{7}\xi^3\ln(1+\frac{1}{\xi}) - \frac{6}{7\sqrt{\xi}}\arctan\sqrt{\xi} \qquad (12)$$

whrer ξ is a non-dimensional length defined as $\frac{3}{2}\frac{k_B v_{ac} L}{\kappa_b \Omega}$. k_B is the Boltzmann constant, v_{ac} is acoustic phonon speed (average of one longitudinal and two transverse acoustic phonon branches in low-frequency limit), L is the thickness of film, κ_b is the bulk thermal conductivity, and Ω is the primitive cell volume. For GaAs/AlAs, which has zinc blende type structure, the primitive cell volume is $a^3/4$, where a is the lattice constant.

2.2. Comparison with experimental data

Although that MQWs and DBR made of different material systems were well developed in semiconductor lasers, however, few experimental data about their conductivities can be found in the early publications. In view of that the structure of a GaAs/AlAs DBR is similar to the superlattice with same materials (i.e., the alternately grown layers in a DBR or superlattice are all of nanoscale, and the only difference between a DBR and superlattice is that layers in superlattice are thinner than in a DBR), the following cited references are all about thermal conductivity of GaAs/AlAs superlattice, and we consider them still significant for comparative studies.

Using the above three methods and following references [15], [16] and [18], we calculate the cross-plane thermal conductivity κ_{CP} and the in-plane thermal conductivity κ_{IP} of GaAs/AlAs superlattices with different thickness (per GaAs or AlAs layer), and the results are shown in Fig. 3 and Fig. 4. When the *method 1* and *method 2* are used, parameter p is chosen to be 0.75, since this value has been found more match the experimental reports of GaAs/AlAs superlattice thermal conductivity [19]. Parameters used in the numerical simulation are listed in table 1. The acoustic phonon speed v is the average of the one longitudinal and two transverse acoustic phonon branches in the low-frequency limit. The bulk thermal conductivity κ of In$_x$Ga$_{1-x}$As is obtained from [19]

$$\kappa = \frac{1}{2.27 + 80.23x - 78.8x^2} \qquad (13)$$

Besides, Others parameters of In$_x$Ga$_{1-x}$As are obtained through linear interpolation of binary alloy. Then the phonon MFP l_0 can be calculated by the formula

$$\kappa = \frac{1}{3}C_v v l_0 \qquad (14)$$

As it can be seen from Fig. 3, thermal conductivities decrease monotonically with decreasing layer thickness of superlattices, consistent with what theories expect. When the layer thickness is smaller than 25nm, results from *method 2* and *3* are almost same and higher than that from *method 1*. Beyond 25nm thickness, *method 1* arise the highest κ_{CP} value and *method 3* corresponds to the lowest one. Comparing to the experimental reference [22], [23] and [24], it can be concluded that *method 3* is more proper for calculating the cross-plane thermal conductivity κ_{CP} of

GaAs/AlAs supperlattices. By the reasons mentioned before, we will choose *method 3* to compute the cross-plane thermal conductivities of GaAs/AlAs DBR and $In_xGa_{1-x}As$ MQWs in this paper.

Table 1. Parameters used in the numerical simulation [19-21]

	GaAs	AlAs	InAs	$In_{0.185}GaAs$
atomic diameter w (nm)	0.248	0.240	0.266	0.251
lattice constant a (nm)	0.56533	0.566139	0.60583	0.57280
density ρ (g/cm^3)	5.31749	3.73016	5.6678	5.3823
acoustic phonon speed v (m/s)	3803	4500	3037	3661
phonon mean free path l_0 (nm)	20.8	37.7	14.8	31.8
Debye temperature T (K)	370	450	280	353
melting point T_m (K)	1513	1740	1210	1457
melting enthalpy H_m (KJ/mol)	120	119.78	58.6	109
specific heat C_v (J/(kg·K))	327	424	352	332
bulk thermal conductivity κ (W/(m·K))	45	91	30	6.94
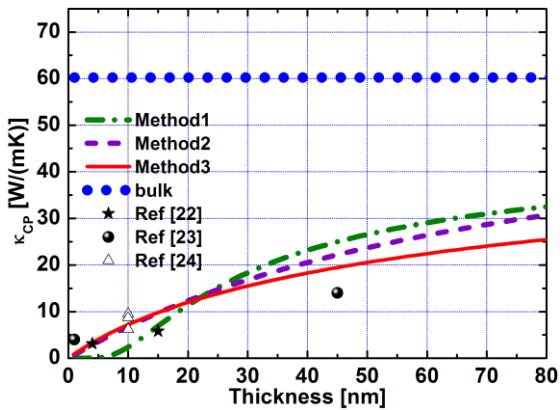
Fig. 3. Cross-plane thermal conductivity κ_{CP} of GaAs/AlAs superlattices with different thickness (per GaAs or AlAs layer)

Fig. 4 shows the in-plane thermal conductivity κ_{IP} of GaAs/AlAs superlattices with different layer thickness. It can be found from Fig. 4 that values obtained from *method 3* are higher than that from *method 1*, and the two curves become closer with increasing layer thickness. However, *method 2* leads to a quite different curve, of which the thermal conductivity decrease sharply when the layer thickness is smaller than 25nm, and very close to the bulk value once the layer thickness exceeds 25nm. This is because *method 2* considers the total thermal conductivity as two parts: ILC and TBR. So for the in-plane thermal conductivity κ_{IP}, obtaining from expression (2), (where the phonon MFP l_0 (20.8nm for GaAs and 37.7nm for AlAs)

plays an important role), when the layer thickness is above the MFP, the nanoscale effects of thermal conductivity is weak and the value is close to that of bulk materials. Similar remarkable difference of *method 2* is not appear in Fig. 3 since when we calculate the cross-plane thermal conductivity κ_{CP}, another main part, TBR, is also included. Even so, the increasing tendency of the curve from *method 2* in Fig. 3 still surpasses the other two obviously. Compared with the experimental references [25] and [26], it is clear that *method 3*, again, is more proper for calculating the in-plane thermal conductivity κ_{IP} of GaAs/AlAs supperlattices among the three methods, and we will use it for the simulation of the κ_{IP} of GaAs/AlAs DBR and $In_xGa_{1-x}As$ MQWs. It should be noted that *method 2* can be improved by generalization for samples large than 20nm using the means proposed by M. Oane et al [27], which is not discussed here.
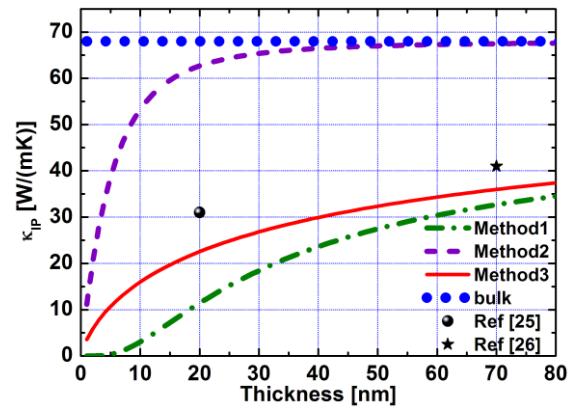
Fig. 4. In-plane thermal conductivity κ_{IP} of GaAs/AlAs superlattices with different thickness (per GaAs or AlAs layer)

3. Thermal conductivity of DRB

By the use of *method 3*, we calculated the in-plane and cross-plane thermal conductivities κ_{IP} and κ_{CP} of GaAs/AlAs DBR for different laser wavelength and the results are presented in Fig. 5, in which the bulk material thermal conductivity κ_{IPb} and κ_{CPb} are also shown. As can be seen from Fig. 5, DBR for shorter wavelength has thinner GaAs and AlAs layer thickness, so has smaller thermal conductivity. For 1μm waveband, calculated in-plane thermal conductivity κ_{IP} is a little bit larger than half of κ_{IPb}, while the cross-plane thermal conductivity κ_{CP} is of approximately 40 percent of κ_{CPb}, and this means that temperature rise will be significantly underestimated in a GaAs/AlAs DBR based semiconductor laser if the bulk thermal conductivity is used. Especially, in an optically pumped SDL, the pump spot is of hundreds of micrometers, which is much larger than the thickness of DRB (typically of a few micrometers), and the heat flows through quasi one-dimension, so the cross-plane thermal conduction becomes dominant and the value of the κ_{CP} should be more accurate in the simulation. For DBR used in a 980nm SDL, thermal conductivity included nanoscale

effects, the κ_{CP}, and the bulk value κ_{CPb}, are 25.3 W/(mK) and 61.9 W/(mK), respectively.
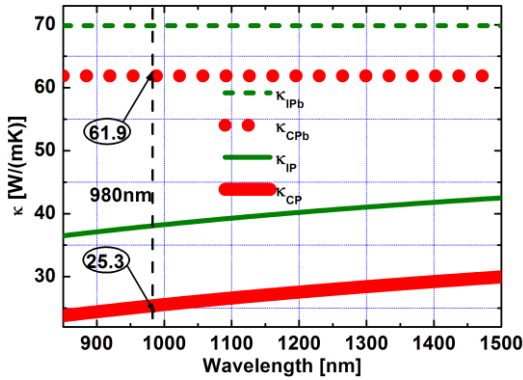
Fig. 5. In-plane and cross-plane thermal conductivity κ_{IP} and κ_{CP} of GaAs/AlAs DBR for different laser wavelength. Bulk material thermal conductivity κ_{IPb} and κ_{CPb} are also shown

4. Thermal conductivity of MQWs

Using *method 3*, calculated In-plane and cross-plane thermal conductivity κ_{IP} and κ_{CP} of 8nm In$_{0.185}$GaAs QWs with different thickness of GaAs barrier are shown in Fig. 6. Thermal conductivity κ_{IPb} and κ_{CPb} of corresponding bulk material are also shown. The marked cross-plane thermal conductivity of 8nm In$_{0.185}$GaAs compressive strain QW with 130nm GaAs barrier (designed for a 980nm SDL) is 16.3W/(mK), less than half of the bulk value of 34.1W/(mK), and this indicates the significant influence of nanoscale effects on the thermal conductivity of MQWs.
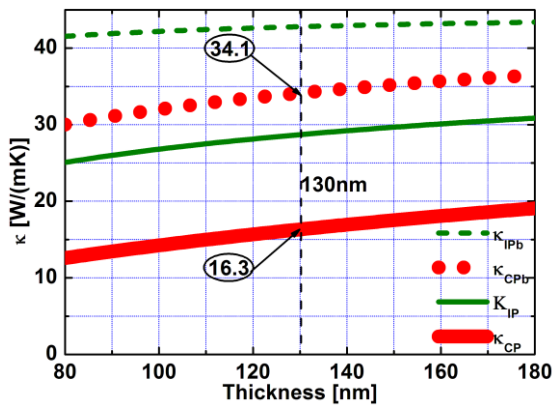
Fig. 6. In-plane and cross-plane thermal conductivity κ_{IP} and κ_{CP} of In$_{0.185}$GaAs QWs with different thickness of GaAs barrier. Thermal conductivity κ_{IPb} and κ_{CPb} of corresponding bulk material are also shown.

5. Example

To certificate how strong the thermal conductivity works on the heat management of a SDL, we compute the temperature rise in the gain chip of a 980nm SDL, and the results are presented in Fig. 7 and Fig. 8. The simulated

gain chip was grown on a 350μm thickness substrate, successively consisted of the DBR (30 pairs of GaAs/AlAs layers), the MQWs active region (16 repeats of 8nm In$_{0.185}$GaAs/GaAs QWs), and a 470nm thickness window layer. The pump power and pump spot radius are assumed to be 10W and 50μm, and quasi one-dimension heat flow is proposed. Detailed computation can be found in reference [13].

Temperature rise shown in Fig. 7 are based on bulk values of thermal conductivities of DBR and MQWs, which are 61.9 W/(mK) and 34.1 W/(mK), respectively. Temperature rise exhibited in Fig. 8 are based on thermal conductivities of DBR and MQWs that considering nanoscale effects, i.e., 25.3 W/(mK) and 16.3W/(mK), as labeled in Fig. 5 and 6. Fig. 7 indicates a maximum temperatures of about 314K, while Fig. 8 shows a maximum temperatures of about 332K, and these data indicate what an underestimation of temperature may be done if bulk values of thermal conductivities are used in the heat management of a SDL.
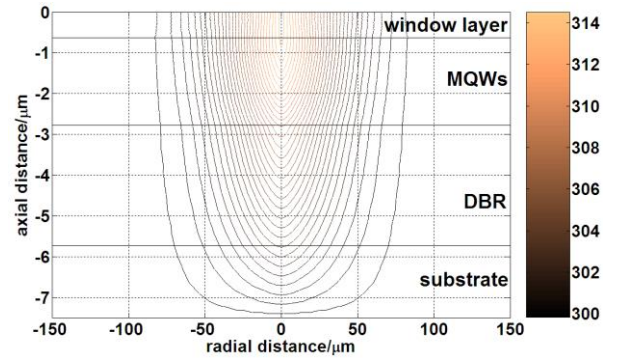
Fig. 7. Simulated temperature rise in a 980nm SDL with 10W pump power and 50μm radius pump spot, bulk value of thermal conductivities are used
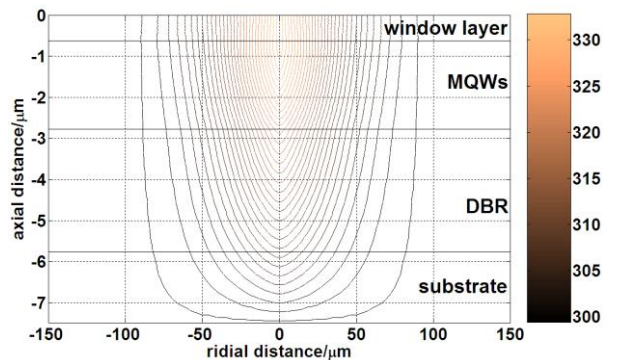
Fig. 8. Simulated temperature rise in a 980nm SDL with 10W pump power and 50μm radius pump spot, thermal conductivities calculated in this work are used

6. Conclusions

By the use of a more proper theoretical method (referred as *method 3* in the text) picked out from three counterparts, we have calculated nanoscale thermal conductivities of the DBR and MQWs in a SDL. For

cross-plane thermal conductivities (which are more concerned in the heat management of a SDL) of the DBR and MQWs, their nanoscale thermal conductivities are less than half of bulk values. The computed data are employed to simulate the temperature rise in a 980nm SDL, and the results indicate that significant underestimation of temperature may be occurred if bulk values of thermal conductivities are used in the heat management of a SDL.

References

[1] M. Kuznetsov, F. Hakimi, R. Sprague, et al., IEEE Journal of Selected Topics in Quantum Electronics. **5**(3), 561 (1999).

[2] B. Rudin, A. Rutz, M. Hoffmann, et al., Optics Letters **33**(22), 2719 (2008).

[3] B. Heinen, T. L. Wang, M. Sparenberg, et al. Electronics Letters **48**(9), 516 (2012).

[4] H. Lindberg, S. Illek, I. Pietzonka, et al. Proceeding of SPIE **7919**, 79190D (2011).

[5] M. Jacquemet, N. Picqué, G. Guelachvili, et al. Optics Letters **32**(11), 1387 (2007).

[6] R. A. Espinosa, G. Filippidis, C. Hamilton, et al. Optics Express **2**(4), 739 (2011).

[7] J. Wagner, S. Hugger, B. Rösener, et al. Proceeding of SPIE **7483**, 74830F (2009).

[8] S. B. Morioka, Proceeding of SPIE **7919**, 791913 (2011).

[9] M. Schulze, A. Masters, Laser Focus World **42**(12), 77 (2006).

[10] S.W. Corzine, R.S. Geels, J.W. Scott, et al. IEEE Journal of Quantum Electronics **25**(6), 1513 (1989).

[11] A. J. Kemp, G.J. Valentine, J. M. Hopkins, et al. IEEE Journal of Quantum Electronics **41**(2), 148 (2005).

[12] H. Lindberg, M. Strassner, E. Gerster, et al. IEEE Journal of Selected Topics in Quantum Electronics **11**(5), 1126 (2005).

[13] P. Zhang, Y. R. Song, X. P. Zhang, et al. Optical Review **18**(4), 317 (2011).

[14] S. L. Vetter, S. Calvez, IEEE Journal of Quantum Electronics **48**(3), 345 (2012).

[15] L. H. Liang, B. Li, Physical Review B **73**(15), 153303 (2006).

[16] F. X. Alvarez, J.A. Quintana, D. Jou, et al. Journal of Applied Physics **107**(8), 084303 (2010).

[17] E. T. Swartz, R.O. Pohl, Review of Modern Physics **61**(3), 605 (1998).

[18] A. J. H. McGaughey, E. S. Landry, D. P. Sellan, et al. Applied Physics Letters **99**(13), 131904 (2011).

[19] L. H. Liang, Y. G. Wei, B. Li, Journal of Applied Physics **103**(8), 084314 (2008).

[20] G. Chen, Physical Review B. **57**(23), 14958 (1998).

[21] S. Adachi, Properties of semiconductor alloys group-IV III-V and II-VI semiconductors. John Wiley & Sons, 2009.

[22] W. S. Capinski, H. J. Maris, Physica B **219**, 699 (1996).

[23] W.S. Capinski, H. J. Maris, T. Ruf, et al. Physical Review B **59**(12), 8105 (1999).

[24] J. Y. Duquesne, Physical Review B **79**(15), 153304 (2009).

[25] T. Yao, Applied Physics Letters **51**(22), 1798 (1987).

[26] X. Y. Yu, G. Chen, A. Verma, et al. Applied Physics Letters **67**(24), 3554 (1995).

[27] M. Oane, F. Scarlat, Shyh-Lin Tsao, et al. Optics & Laser Technology **39**(4), 796 (2007).

_____
*Corresponding author: zhangjgjs@163.com